Title
Anterior temporal lobe degeneration produces widespread network-driven dysfunction

Journal
Brain, 136(10)

ISSN
0006-8950

Authors
Guo, Christine C
Gorno-Tempini, Maria Luisa
Gesierich, Benno
et al.

Publication Date
2013-10-01

DOI
10.1093/brain/awt222

Peer reviewed

doi:10.1093/brain/awt222 Brain 2013: 136; 2979–2991 | 2979

BRAIN
A JOURNAL OF NEUROLOGY

Anterior temporal lobe degeneration produces widespread network-driven dysfunction

Christine C. Guo,[1] Maria Luisa Gorno-Tempini,[1,2] Benno Gesierich,[1,2] Maya Henry,[1] Andrew Trujillo,[1] Tal Shany-Ur,[1] Jorge Jovicich,[2] Simon D. Robinson,[3] Joel H. Kramer,[1] Katherine P. Rankin,[1] Bruce L. Miller[1] and William W. Seeley[1]

1. Memory and Ageing Centre, Department of Neurology, University of California, San Francisco, USA
2. Centre for Mind/Brain Sciences, University of Trento, Rovereto 38068, Italy
3. High Field MR Centre of Excellence, Department of Radiology, Medical University of Vienna, Austria

Correspondence to: William W. Seeley, MD
Box 1207,
University of California, San Francisco
San Francisco, CA 94143-1207, USA
E-mail: wseeley@memory.ucsf.edu

The neural organization of semantic memory remains much debated. A 'distributed-only' view contends that semantic knowledge is represented within spatially distant, modality-selective primary and association cortices. Observations in semantic variant primary progressive aphasia have inspired an alternative model featuring the anterior temporal lobe as an amodal hub that supports semantic knowledge by linking distributed modality-selective regions. Direct evidence has been lacking, however, to support intrinsic functional interactions between an anterior temporal lobe hub and upstream sensory regions in humans. Here, we examined the neural networks supporting semantic knowledge by performing a multimodal brain imaging study in healthy subjects and patients with semantic variant primary progressive aphasia. In healthy subjects, the anterior temporal lobe showed intrinsic connectivity to an array of modality-selective primary and association cortices. Patients showed focal anterior temporal lobe degeneration but also reduced physiological integrity throughout distributed modality-selective regions connected with the anterior temporal lobe in healthy controls. Physiological deficits outside the anterior temporal lobe correlated with scores on semantic tasks and with anterior temporal subregion atrophy, following domain-specific and connectivity-based predictions. The findings provide a neurophysiological basis for the theory that semantic processing is orchestrated through interactions between a critical anterior temporal lobe hub and modality-selective processing nodes.

Keywords: anterior temporal lobe; semantic dementia; cognition; semantics; functional neuroimaging

Abbreviations: ATL = anterior temporal lobe; ALFF = amplitude of low-frequency fluctuation; PPA = primary progressive aphasia; TASIT = The Awareness of Social Inference Test

Introduction

Semantic knowledge reflects human conceptions about objects, words, people, and emotions and enables us to choose behaviours within a richly specified context. The neural organization of semantic knowledge has been vigorously studied yet remains controversial (Martin, 2007; Patterson *et al*., 2007; Mahon and Caramazza, 2008; Binder *et al*., 2009; Gainotti, 2011), in part due to the conflict between two major conceptual models. Functional neuroimaging studies in healthy subjects have led some authors to suggest that semantic representations are embedded within a widely distributed neural network, composed of modality-selective

Received September 27, 2012. Revised June 4, 2013. Accepted June 5, 2013

regions that process visual, auditory, tactile and other sensory or motor features. Multimodal semantic constructs of an object, for example, would be represented in regions responsible for that object's perception or related actions (Martin, 2007). This 'distributed-only' model receives further support from patients with modality-selective agnosias caused by focal lesions of these distributed cortical regions. In contrast, findings from patients with semantic variant primary progressive aphasia (PPA, previously referred to as semantic dementia) challenge the 'distributed-only' model (Garrard and Hodges, 2000). Patients with semantic variant PPA demonstrate progressive erosion of semantic knowledge across modalities and categories despite relative preservation of other cognitive abilities (Garrard and Hodges, 2000; Patterson *et al*., 2007); these semantic deficits are associated with atrophy and hypometabolism that remain localized to the bilateral anterior temporal lobes (ATLs) without involving modality-selective regions until late in the disease course (Mummery *et al*., 2000; Chan *et al*., 2001; Rosen *et al*., 2002; Diehl *et al*., 2004). Thus, semantic variant PPA highlights a critical role for the ATL in semantic processing, leading to the proposal that this region serves to integrate upstream modality-selective information.

Building further on observations from semantic variant PPA, more recent models have proposed a framework that emphasizes co-operation between distributed modality-selective regions and an amodal ATL 'semantic hub'. According to this view, attributes such as sensory, motor and linguistic features are encoded and re-represented by distributed upstream regions, whereas unitary semantic concepts require convergence of multi-modal representations within the amodal ATL hub (McClelland and Rogers, 2003; Patterson *et al*., 2007). One early study provided some evidence for this model by showing hypometabolism extending beyond the ATL hub into posterior temporal regions in semantic variant PPA (Mummery *et al*., 2000). Based on the 'hub + distributed node' framework, we predicted that the ATL would show intrinsic connectivity to a wide array of upstream modality-selective regions and that damage to the ATL would disrupt functional integrity throughout these upstream network nodes. Neither of these model-based predictions has received adequate empirical support to date.

Here, we used a multidisciplinary approach to examine the neural architecture of semantic processing, combining structural MRI, task-free ('resting state') functional MRI, and neuropsychological assessment in healthy subjects and patients with semantic variant PPA. Building upon the integrated semantic framework, we designed our study to examine these hypotheses: (i) the ATLs should be functionally connected to distributed modality-selective regions; (ii) a focal ATL lesion should disrupt connectivity and functional integrity in widespread ATL-anchored network nodes; (iii) node-specific dysfunction should correlate with aspects of semantic processing related to established functions of that node; and (iv) subregion-specific ATL damage should produce nodal dysfunction consistent with known ATL anatomical connections to modality-selective regions. Our results provide novel neurophysiological evidence that supports and extends the theoretical framework proposed by Patterson *et al*. (2007) and clarifies the neural architecture supporting human semantic processing.

Materials and methods

Subjects

Control subjects

Twenty-seven healthy older control subjects (HC1; 12 females; aged 49–73 years) were selected from the University of California, San Francisco (UCSF) Memory and Ageing Centre database. To validate our findings in HC1, we further studied 23 non-overlapping healthy controls (HC2; 14 females; aged 19–62 years) scanned with an ATL-optimized echo planar imaging protocol. Finally, to compare with the semantic variant PPA group, 17 healthy older controls (HC3; eight females; aged 55–73 years) were selected, who were matched to each patient for age, gender and handedness. HC1 and HC3 subjects did not overlap; they were recruited from the San Francisco community through advertisements as described previously (Rosen *et al*., 2002). All were required to have a Clinical Dementia Rating scale total score of 0, a Mini-Mental State Examination score of 28 or higher, no significant history of neurological disease or structural lesion on MRI, and a consensus diagnosis of cognitively normal within 90 days of their MRI scan (Table 1). All HC2 subjects were recruited and scanned at the Centre for Mind and Brain 80 (CIMeC, Italy). Because control subjects who underwent MRI with the same protocol used in patients (HC3) did not undergo the complete language battery, a separate control group ('CogHC', see Table 1) was used to document deficits in semantic processing in patients with semantic variant PPA. All participants were right-handed, reported no history of head injury or other neurological illness (Gesierich *et al*., 2012), and gave written informed consent to participate following procedures approved by the relevant institutional review boards (HC1 and HC3, University of California, San Francisco, USA; HC2, University of Trento, Italy).

Patients

The semantic variant PPA group consisted of 17 patients, representing all patients in the UCSF database who (i) had successful structural and functional MRI acquisition; (ii) received a research diagnosis of semantic variant PPA based on published criteria (Gorno-Tempini *et al*., 2011) within 90 days of MRI; (iii) had no significant history of other neurological disease; and (iv) were right-handed. Two patients were excluded due to excessive movement (>2.5 mm maximum translational movement during task-free functional MRI) and two were excluded due to left-handedness. Patients underwent a thorough clinical evaluation including a history, general neurological examination by a staff behavioural neurologist, Clinical Dementia Rating, Mini-Mental State Examination, and a bedside neuropsychological screen at the UCSF Memory and Ageing Centre within 90 days of scanning. All subjects or their surrogates provided informed consent before participation, and all study procedures were approved by the UCSF institutional review board.

Neuropsychological assessment

Most UCSF healthy controls (HC1 and HC3) and patients were evaluated with a comprehensive neuropsychological assessment within 90 days of scanning (Table 1) (Rosen *et al*., 2002; Rankin *et al*., 2009). Language screening included the abbreviated Boston Naming Test (15 items) (Kaplan *et al*., 1983), Peabody Picture Vocabulary Test (Dunn, 1970), Pyramid and Palm Trees Test (Howard and Patterson, 1992), single-word reading (Beeson *et al*., 2010), and semantic (number of

Table 1 Demographics and clinical assessments

	HC1		HC3		Semantic variant PPA		HC3 – svPPA
	Mean (SD)	*n*	Mean (SD)	*n*	Mean (SD)	*n*	*P*-value
Age, years	66.2 (6.3)	27	63.6 (5.8)	17	63.4 (6.1)	17	0.915
Gender (M:F)	15:12		9:8		9:8		–
Education, years	17.2 (1.8)	27	17.1 (1.8)	17	16.9 (2.6)	17	0.817
CDR total	0.0 (0.0)	27	0.0 (0.0)	17	0.7 (0.4)	17	<0.001
CDR, sum of boxes	0.0 (0.0)	27	0.0 (0.1)	17	4.1 (2.8)	17	<0.001
MMSE (max 30)	29.4 (0.7)	27	29.6 (0.7)	17	26.4 (2.3)	17	<0.001
BNT (max 15)	14.5 (0.8)	27	14.5 (0.7)	17	6.1 (4.1)	17	<0.001
PPVT (max 16)	15.7 (0.7)	23	15.8 (0.5)	16	8.2 (4.4)	16	<0.001
TASIT (max 14)	11.7 (1.6)	14	12.0 (0.8)	4	6.8 (2.6)	17	<0.001
Lexical fluency (D-words per minute)	17.2 (3.3)	22	17.3 (3.4)	11	6.9 (3.3)	17	<0.001
Category fluency (animals per minute)	24.1 (5.4)	27	23.3 (5.1)	17	8.2 (3.8)	17	<0.001
Modified trails (correct lines/min)	24.2 (9.9)	27	23.9 (7.9)	17	47.1 (26.7)	15	0.005
Digit span (forward)	7.7 (1.0)	15	7.4 (1.1)	15	6.6 (1.4)	15	0.089
Digit span (backward)	6.0 (1.0)	27	5.3 (1.4)	16	4.9 (1.0)	16	0.323
Calculations (max 5)	4.9 (0.4)	27	4.7 (0.5)	17	4.6 (0.5)	16	0.636
Syntax (max 5)	4.9 (0.3)	23	4.8 (0.4)	16	4.5 (0.6)	15	0.087
Head translation, mm	0.29 (0.16)	27	0.27 (0.14)	17	0.24 (0.12)	17	0.447
Head rotation (°)	0.11 (0.05)	27	0.11 (0.07)	17	0.12 (0.10)	17	0.556
	Cog HC						**Cog HC versus svPPA**
Age	65.5 (3.0)						0.2
Gender (M:F)	10:7						–
Education	16.8 (2.2)						0.9
PPT (max 52)	51.5 (0.6)			17	43.1 (6.5)	17	<0.001
Reading (max 100)							
Regular words	100.0 (0.0)			15	95.8 (7.5)	15	0.08
Irregular words	99.8 (0.66)			15	75.3(22)	15	<0.001

Shaded areas highlight measures for which patients with semantic variant PPA differ significantly from healthy controls ($P < 0.005$, two sample *t*-test).
CDR = Clinical Dementia Rating; MMSE = Mini-Mental State Examination; BNT = Boston Naming Test; PPVT = Peabody Picture Vocabulary Test; svPPA = semantic variant PPA; PPT = Pyramids and palm tree – Pictures.

animals/1 min) and phonemic (number of D words/1 min) word generation. Forward and backward digit span and a Modified trails test assessed executive functioning. Ability to perform five arithmetic calculations also was assessed. Emotion recognition was assessed with an abbreviated form of the Emotion Evaluation Subtest of 'The Awareness of Social Inference Test' (TASIT) (Mcdonald *et al*., 2007). As described previously, subjects watch brief (~20 s) videos of actors performing semantically neutral scripts portraying one of the seven basic emotional states (happy, surprised, neutral, sad, anxious, frightened, revolted), and must choose the correct emotion from the seven options (Rankin *et al*., 2009). Task performance of patients was compared with healthy controls (HC3) using two-sample *t*-tests.

Image acquisition

University of California, San Francisco data set

Structural and functional magnetic resonance images of UCSF healthy controls (HC1 and HC3) and patients were acquired at the UCSF Neuroscience Imaging Centre, on a 3 T Siemens Tim Trio scanner equipped with a 12-channel receiver head coil. A volumetric MP-RAGE sequence was used to obtain T_1-weighted images of the entire brain (repetition time/echo time/inversion time = 2300/3/900 ms, flip angle of 9°, a bandwidth of 240 Hz/pixel, capital orientation with a field of view = 256 × 240 mm and 160 slices). Task-free functional MRI scans were obtained using 36 axial slices (3-mm thick) parallel to the plane connecting the anterior and posterior commissures and covering the whole brain using a T_2*-weighted gradient echo–echo planar sequence (repetition time/echo time = 2000/27 ms, flip angle 80°; field of view = 230 × 230 mm; matrix size = 92 × 92; 3 mm slices with 2.5 × 2.5 × 3 mm resolution; slice gap = 0.6 mm). All subjects underwent 8 min of scanning (240 images) after being instructed to remain awake with their eyes closed.

Trento data set

Structural and functional MRI of Trento healthy controls (HC2) were acquired at the University of Trento, on a 4 T MRI scanner (Bruker Medical) equipped with a birdcage transmit, 8-channel receiver head RF coil. This data set has been described previously (Gesierich *et al*., 2012). Structural images were acquired using a 3D MP-RAGE optimized for grey–white matter contrast, with repetition time/echo time/inversion time = 2700/4.18/1020 ms, flip angle = 7°, 1 × 1 × 1 mm^3. Task-free functional MRI scans were obtained with an echo planar imaging protocol in which parameters were optimized for the ATL (repetition time/echo time = 2000/21 ms; flip angle = 75°; field of view = 192 × 192 mm; 2 mm slices with 3 × 3 × 2 mm resolution; 43 axial slices oriented ~–20° relative to the plane connecting the anterior and posterior commissures and approximately parallel to the longitudinal axis of the temporal lobes; slice gap = 0.3 mm). This parameter optimization has been shown to substantially increase blood oxygen

level-dependent sensitivity for detecting task-based activation (Gesierich *et al*., 2012) and functional-connectivity in the ATLs (Robinson *et al*., 2009). Full-brain coverage was not possible with this optimized echo planar imaging protocol; the upper ~2 cm of the brain were not imaged. All subjects underwent 10 min of scanning (300 images) after being instructed only to remain awake with their eyes closed.

Image preprocessing and analysis

Structural imaging

T_1-weighted images were segmented into grey and white matter using VBM8. Custom templates were separately created for the HC1 group, the HC2 group, and for the semantic variant PPA and HC3 groups together, using the DARTEL toolbox. For semantic variant PPA and HC3 groups, the grey matter images were further normalized into Montreal Neurological Institute (MNI) space, modulated, and smoothed with an 8 mm full-width at half-maximum Gaussian kernel. These resulting images were subsequently entered into a second-level, random-effects voxel-based morphometry analysis to perform a two-sample *t*-test to identify between-group differences or were used as nuisance covariates for voxel-wise atrophy correction of functional imaging comparisons between the semantic variant PPA and HC3 groups, as described below. The group-difference map from voxel-based morphometry analysis was evaluated with a peak height threshold [family-wise error (FWE)-corrected $P < 0.05$; Fig. 2C and Supplementary Fig. 2].

Functional imaging

After discarding scans acquired in the first 16 s to allow for quasi-equilibrium in longitudinal magnetization to be achieved, functional images were realigned and unwarped, slice-time corrected, co-registered, spatially normalized to standard space and smoothed with a 4 mm full-width at half-maximum Gaussian kernel using SPM8. Unwarping was performed to reduce artefacts due to movement-by-deformation interactions. Co-registration was performed between the mean echo planar images and the subject's own T_1-weighted image, and normalization and smoothing were carried out in one step using the DARTEL toolbox. Subsequently, the functional images were resampled at a voxel size of $2\,mm^3$. These preprocessed images were then used for seed-based region of interest and fractional amplitude of low-frequency fluctuation (ALFF) analyses, as described below.

Head motion assessment

The motion parameters estimated in the process of realignment were used to compute the magnitude of head motion during each scan. Based on the volume-to-volume changes in motion parameters, mean root-mean-square values were calculated for translation and mean Euler angles for rotation, as these summary metrics have been shown to correlate with network connectivity strength (Van Dijk *et al*., 2011). Two-sample *t*-tests confirmed that the semantic variant PPA and HC3 groups did not differ in translational or rotational movement (Table 1).

Seed-based region of interest analyses

For each subject, voxel-wise connectivity maps were derived using two seeds: the right and left ATLs. The left ATL seed was a 4-mm spherical region of interest centred at (−44, 14, −25, the peak of the second most atrophied cortical region in semantic variant PPA identified in a different cohort) (Seeley *et al*., 2009). We chose the second most atrophied region because the most atrophied area fell within the most severe signal dropout zone. The right ATL seed was the mirror image of the left ATL seed, a 4-mm spherical region of interest at (44, 14, −25). Intrinsic connectivity maps representing bilateral ATL connectivity were derived in three steps:

(i) Left and right ATL seeds were used in separate seed-based region of interest analyses, following previous methods (Seeley *et al*., 2009). Briefly, after temporal filtering with a band-pass filter ($0.0083 < f < 0.15$ Hz), the average voxel-wise time series from each region of interest was de-trended and used as a covariate of interest in a whole-brain, linear regression, statistical parametric analysis. This procedure generated a statistical parametric map from each scan session, where each voxel was scored based on its blood oxygen level-dependent signal correlation with the seed region of interest used in the analysis (henceforth referred to as 'connectivity'). White matter, CSF, non-brain (voxels that are not grey matter, white matter or CSF) time series and six motion parameters were included as nuisance regressors, as shown to produce reliable functional connectivity measures (Guo *et al*., 2012).

(ii) For each subject, the right and left ATL-seeded statistical parametric maps were averaged.

(iii) The averaged map for each subject was entered into second-level, random-effects analyses to generate group-level connectivity maps, a two-sample *t*-test identifying between-group differences, and regression analyses seeking brain–behaviour relationships. The statistical map from the two-sample *t*-test was masked explicitly to the relevant network by binarizing the intrinsic connectivity network derived from HC1.

ATL connectivity to the sensory and motor regions was confirmed with 'reverse seeding'. Based on the ATL-seeded intrinsic connectivity network network from HC1 (Fig. 1A), we identified the most significant clusters in the left and right calcarine, Heschl's, precentral and postcentral gyri. We then created one seed from each cluster—a 4-mm spherical region of interest centred at the coordinate of the cluster peak, resulting in four pairs (left and right) of seeds corresponding to primary visual, auditory, somatosensory and motor cortices. These seeds were then applied to an independent data set (HC3) to derive four intrinsic connectivity network maps using the same approach used to generate the ATL-seeded intrinsic connectivity networks.

Fractional amplitude of low-frequency fluctuation analysis

Fractional ALFF analysis was performed using the REST toolbox, following previous methods (Zou *et al*., 2008). After preprocessing, each voxel's blood oxygen level-dependent signal time series was de-trended and transformed to the frequency domain to obtain the power spectrum. The power of a given frequency is measured as the square of the amplitude at each frequency of the power spectrum. The average square root across 0.01–0.08 Hz was taken as the ALFF. Further, fractional ALFF was computed by dividing the sum of the square roots across the 0.01–0.08 Hz range by that across the entire frequency range (0–0.25 Hz), representing the fractional blood oxygen level-dependent power at low-frequency. Fractional ALFF has been shown to be less sensitive to physiological noise than ALFF (Zou *et al*., 2008). Fractional ALFF maps for each subject were entered into second-level, random-effects analyses to perform two-sample *t*-tests and regression analyses.

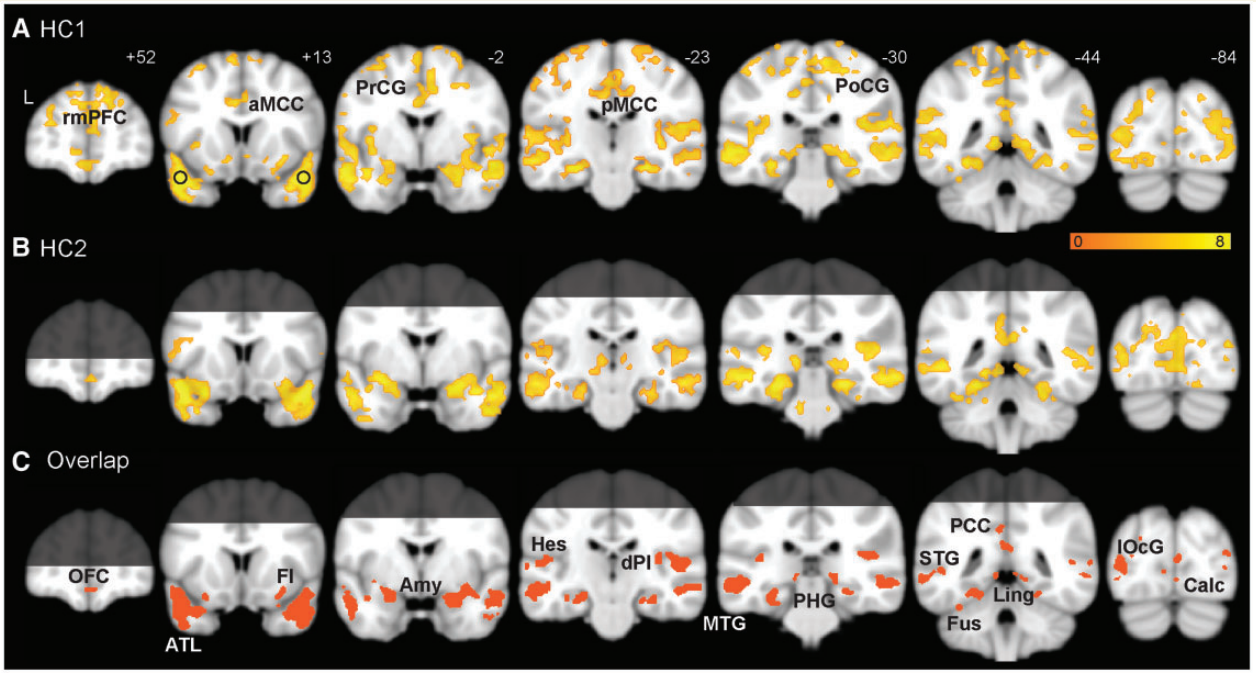

Figure 1 Intrinsic ATL connectivity in the healthy brain. Group-level ATL-seeded intrinsic connectivity network maps are shown for HC1 (**A**), HC2 (**B**), and their overlap (**C**), generated with a joint height-extent threshold ($P < 0.0001$ for peak height and FWE-corrected $P < 0.05$ for spatial extent). Brain regions beyond the coverage of the optimized EPI protocol are shaded in **B** and **C**, and thus only labelled in **A**. Black circles in **A** signify the location of the ATL seeds. Amy = amygdala; aMCC = anterior midcingulate cortex; Calc = calcarine; dPI = dorsal posterior insula; FI = frontoinsula; Fus = fusiform; Hes = Heschl's; Ling = lingual gyrus; lOcG = lateral occipital gyrus; MTG = middle temporal gyrus; OFC = orbitofrontal cortex; PCC = posterior cingulate cortex; pMCC = posterior midcingulate cortex; PCu = precuneus; PHG = parahippocampus; PoCG = postcentral gyrus; PrCG = precentral gyrus; rmPFC = rostral medial prefrontal cortex; STG = superior temporal gyrus.

Statistical thresholding for whole-brain functional image analyses

Whole-brain analyses were thresholded using a joint probability distribution method to correct for multiple comparisons (Poline *et al*., 1997). In HC1 and HC2, group-level connectivity maps were generated with a threshold of $P < 0.0001$ for height and family-wise error-correction for $P < 0.05$ for cluster extent (Table 2). A generous threshold ($P < 0.001$ for height and family-wise error-correction for $P < 0.05$ for cluster extent) was applied to the HC1 result to create the explicit mask used in the two-sample *t*-test on intrinsic connectivity network maps. Group differences in functional maps (semantic variant PPA < HC3 and semantic variant PPA > HC3) were evaluated with a threshold of $P < 0.01$ for height and $P < 0.05$ for extent (Fig. 2A–C), or with a more liberal threshold to illustrate convergent results across methods ($P < 0.05$ for height and extent; Fig. 2C). To further examine whether and how observed group differences in functional maps were related to grey matter atrophy, they were reassessed with voxel-wise grey matter intensity maps as covariates, using the Biological Parametric Mapping (BPM) toolbox (Casanova *et al*., 2007). The clusters identified in analyses with and without atrophy correction are reported in Supplementary Tables 1 and 2.

Function–behaviour correlation

Among the significant clusters identified in the fractional ALFF analysis (semantic variant PPA < HC3, $P < 0.05$ for height and extent), six regions of interest were selected: right anterior insula, anterior cingulate, and orbital frontal cortices, left fusiform and superior temporal gyri and calcarine sulcus. Mean fractional ALFF of all voxels within each region of interest was computed and entered into correlation analyses with Peabody Picture Vocabulary Test and TASIT scores controlling for age and gender. To further examine whether these correlations were related to regional atrophy, they were reassessed controlling for the mean grey matter intensities within each region of interest, in addition to age and gender. These correlations with and without atrophy correction are reported in Table 3.

Structure–function correlation

Based on the fractional ALFF group-difference map (semantic variant PPA < HC3, $P < 0.05$ for height and extent), we extracted regions of interest from the calcarine sulcus (primary visual) and fusiform (visual association), Heschl's (primary auditory), and superior temporal gyri (auditory association) from each hemisphere, using the WPU pickatlas toolbox (Maldjian *et al*., 2003). Eight regions of interest (four from each hemisphere) were thus defined and then slightly dilated, using the 3D dilation function (factor of 1). Mean fractional ALFF within each region of interest was computed for each patient with semantic variant PPA. These fractional ALFF measures were then entered into voxel-based morphometry regression analyses seeking voxels whose grey matter intensity was related to functional integrity of the region of interest. Fractional ALFF values from visual and auditory cortices were included as orthogonalized covariates of interest in the model, and age and gender as nuisance covariates. Four separate models were constructed for primary and association cortices in the left and right

Table 2 Brain regions connected to the ATLs

	Region	Size/voxel	
		Left	Right
Primary	Postcentral gyrus*	469	326
	Precentral gyrus*	401	319
	Calcarine	349	117
	Heschl's	34	50
	Posterior insula	23	28
Modality-selective	Cuneus	117	123
	Lingual	157	83
	Middle occipital gyrus	312	98
	Inferior temporal gyrus	55	105
	Middle temporal gyrus	1280	959
	Superior temporal gyrus	189	255
Transmodal	Inferior frontal gyrus, triangular	84	216
	Inferior orbital gyrus	–	93
	Anterior cingulate cortex*	92	106
	Midcingulate cortex*	625	583
	Posterior cingulate cortex	105	25
	Frontal/mid-insular cortex	35	40
	Amygdala	59	100
	Precuneus	176	171
	Angular gyrus	67	49
	Middle temporal pole	107	195
	Superior temporal pole	245	309
	Fusiform	175	67
	Parahippocampal gyrus	94	95
	Hippocampus	140	128

Anatomical regions were identified with AAL atlas using wickpickatlas toolbox, and classified as primary, unimodal heteromodal according to the parcellation scheme of Mesulam (2000). Cluster size is the number of voxels in the overlapping ATL-seeded ICN (Fig. 1C) belonging to each brain region in the left or the right hemisphere. Only regions with >20 voxels are listed.
*For regions outside the coverage of the ATL-optimized EPI protocol (dorsal cerebrum), clusters were taken from the HC1 group-level ICN map (Fig. 1A).

hemisphere, where the search volume in each analysis was restricted to the ipsilateral ATL. Clusters significantly related to fractional ALFF scores were identified with a threshold of $P < 0.01$ for height and $P < 0.05$ for extent. The clusters correlated with the right Heschl's and superior temporal gyrus regions of interest were further thresholded at a peak height $P < 0.005$ to illustrate the most significant portion.

Results

The healthy anterior temporal lobes anchor a network that includes distributed modality-selective cortices

First, in healthy controls, we used task-free functional MRI to identify an ATL-anchored intrinsic connectivity network (Seeley *et al*., 2009). Task-free functional MRI has recently been developed to estimate intrinsic functional connectivity among brain regions, quantify local functional oscillations, and detect disease-related functional abnormalities (Greicius, 2008; Seeley *et al*., 2009; Castellanos *et al*., 2009; Zhang and Li, 2010; Pievani *et al*., 2011). To avoid magnetic susceptibility artefacts near air–bone interfaces, we located the ATL seeds superior and lateral to the most artefact-prone regions. In addition, we pursued the ATL-anchored intrinsic connectivity network using two acquisition protocols, a standard protocol providing whole-brain coverage (HC1, see Table 1 for demographic details) and an ATL-optimized protocol (HC2) that improves ATL signal-to-noise ratio but sacrifices coverage of the dorsal cerebrum (Gesierich *et al*., 2012). With both acquisition protocols, each brain voxel's functional time series was correlated with the left and right ATL seed time series separately, providing two correlation measures that were then averaged to render a bilateral ATL connectivity map for each subject. These subject-level maps were entered into a random-effects model to derive the group-level ATL-seeded intrinsic connectivity network (Fig. 1A, HC1; Fig. 1B, HC2; $P < 0.0001$ for peak height, $P < 0.05$, FWE-corrected for multiple comparisons at the cluster level). Intrinsic connectivity networks derived from the two acquisition protocols were largely overlapping (Fig. 1C). The ATL-anchored intrinsic connectivity network featured an array of sensory and motor regions, including primary cortices [calcarine sulcus, Heschl's gyrus, pre- and postcentral gyri, and dorsal posterior insula (or, primary interoceptive cortex; Craig, 2002)]; modality-selective association cortices (lingual, lateral occipital, fusiform, superior and middle temporal gyri); and heteromodal association cortices; as well as corticoid, allocortical, peri-allocortical, and subcortical regions (amygdala, frontoinsula, orbital frontal cortex, anterior cingulate cortex, posterior cingulate cortex, parahippocampus/hippocampus, ventral striatum, and thalamus) (Fig. 1 and Table 2) that represent emotional, hedonic, motivational and memory-related aspects of ambient stimuli (Mesulam, 2000). Intrinsic connectivity between the ATL and primary sensory and motor cortices was further confirmed by a 'reverse seeding' experiment, in which the sensory and motor cortices linked to the ATL in HC1 (Fig. 1A) were used to seed intrinsic connectivity analyses in an independent data set (HC3) and showed convergent connectivity to the lateral ATL (Supplementary Fig. 1). Overall, the pattern of ATL intrinsic connectivity resembles the regional activation pattern seen as subjects perform semantic tasks. Intrinsic connectivity between two regions neither requires nor implies direct axonal connectivity between those regions (Vincent *et al*., 2007); nonetheless, several major nodes of this network show robust interconnections with the ATL in the non-human primate brain (Morán *et al*., 1987).

Patients with semantic variant primary progressive aphasia show loss of semantic knowledge and bilateral anterior temporal lobe atrophy

Consistent with previous studies (Garrard and Hodges, 2000; Patterson *et al*., 2007), patients with semantic variant PPA showed relatively circumscribed deficits in semantic processing, performing significantly worse than control subjects on the 15-item Boston Naming Test, Peabody Picture Vocabulary Test,

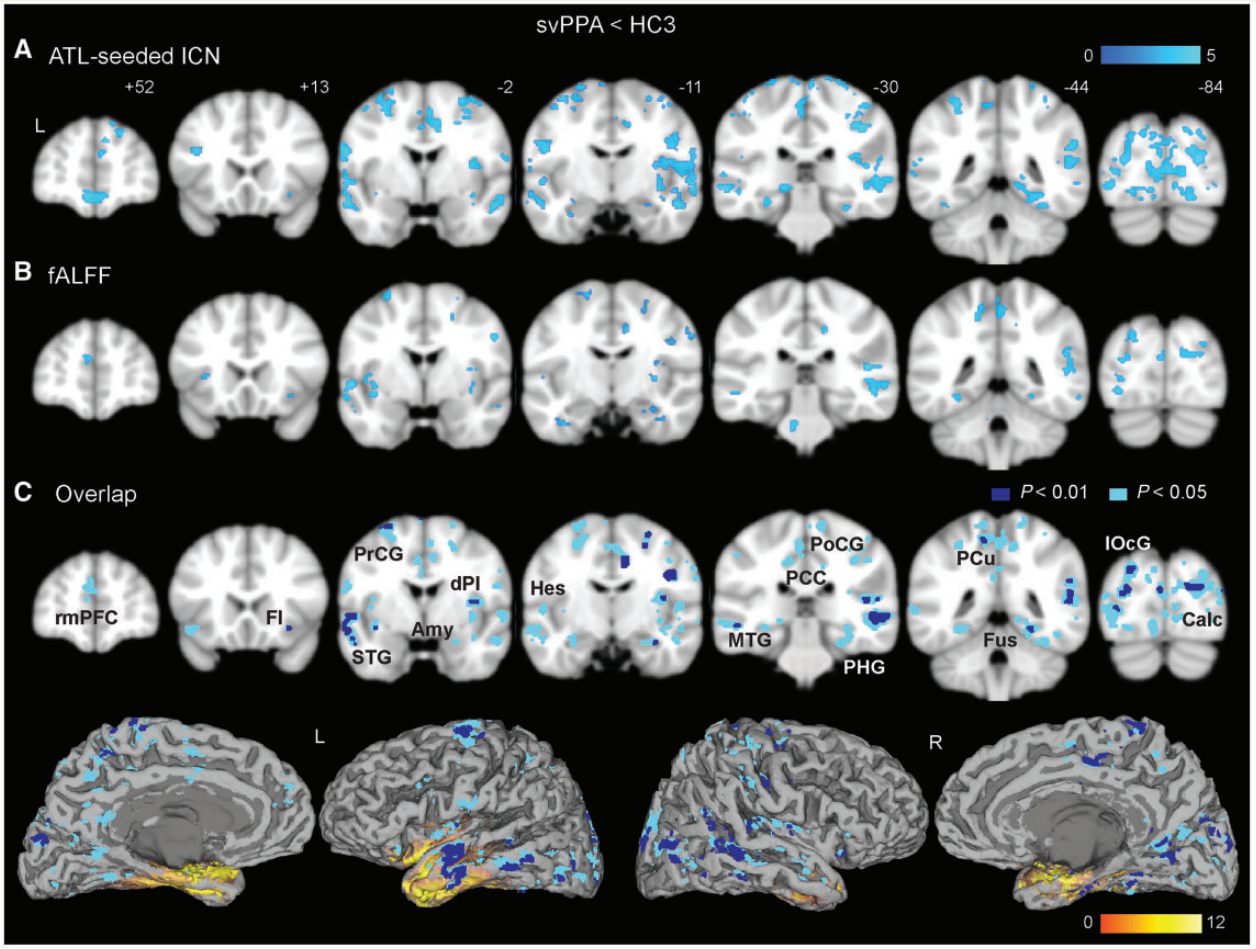

Figure 2 Semantic variant PPA (svPPA) shows distributed reductions in intrinsic connectivity and local functional brain activity. Group difference maps (semantic variant PPA < HC3) from ATL-seeded intrinsic connectivity (**A**) and fractional ALFF (fALFF, **B**) analyses were generated with a joint height-extent threshold ($P < 0.01$ for peak height and $P < 0.05$ for spatial extent). The overlap between the intrinsic connectivity network (ICN) and fractional ALFF group-difference maps is shown in **C** with two statistical thresholds chosen to illustrate the convergence of the findings [$P < 0.05$ (light blue) or $P < 0.01$ (dark blue) for peak height, and $P < 0.05$ for spatial extent]. Overlap maps are also visualized on a rendered brain surface using mri3dX (http://www.cubric.cf.ac.uk/Documentation/mri3dX/), where atrophied regions from the semantic variant PPA < HC3 voxel-based morphometry analysis (Supplementary Fig. 2) are highlighted in yellow. Amy = amygdala; Calc = calcarine; dPI = dorsal posterior insula; FI = frontoinsula; Fus = fusiform; Hes = Heschl's; lOcG = lateral occipital gyrus; MTG = middle temporal gyrus; PCC = posterior cingulate cortex; PCu = precuneus; PHG = parahippocampus; PoCG = postcentral gyrus; PrCG = precentral gyrus; rmPFC = rostral medial prefrontal cortex; STG = superior temporal gyrus.

TASIT Emotion Evaluation Subtest, and lexical and category fluency measures despite normal results on tests of working memory, calculation, and syntax ($P < 0.005$, two-sample *t*-test; Table 1). Deficits on the Pyramid and Palm Trees Test (Pictures subtest) and irregular, but not regular, word reading (indicating surface dyslexia) provided further evidence for semantic loss in these patients. Voxel-based morphometry revealed atrophy involving the bilateral ATLs and amygdala, hippocampus, parahippocampal and fusiform gryi, medial orbital frontal cortex, and ventral anterior and mid-insula, with greater severity on the left side (FWE-corrected $P < 0.05$; Fig. 2C and Supplementary Fig. 2). In keeping with previous reports (Mummery *et al.*, 2000; Chan *et al.*, 2001; Desgranges *et al.*, 2007), no significant atrophy was detected in modality-selective primary or association cortices.

Semantic variant primary progressive aphasia is associated with reduced anterior temporal lobe connectivity and local functional oscillation power in primary and modality-selective cortices

To delineate the regions showing intrinsic connectivity reductions in semantic variant PPA, bilateral ATL-seeded connectivity maps were derived for patients with semantic variant PPA and their age-matched healthy controls (HC3, see Table 1 for demographics), as described above for the HC1 and HC2 groups. Compared with HC3, patients with semantic variant PPA showed extensive ATL connectivity disruptions, including primary cortices [calcarine

Table 3 Function-behaviour correlation

R^2 (*P*-value)	Group I			Group II		
	MTG	Fus	Calc	FI	Medial OFC	pregenual ACC
PPVT	0.378 (0.016)	0.289 (0.032)	0.494 (0.002)	0.106 (0.219)	0.032 (0.517)	0.001 (0.934)
PPVT*	0.273 (0.046)	0.118 (0.211)	0.482 (0.004)	0.178 (0.118)	0.015 (0.673)	0.017 (0.640)
TASIT	0.176 (0.094)	0.131 (0.153)	0.081 (0.296)	0.511 (0.003)	0.375 (0.009)	0.257 (0.038)
TASIT*	0.277 (0.053)	0.019 (0.229)	0.027 (0.303)	0.370 (0.016)	0.364 (0.017)	0.312 (0.030)

*Results after atrophy correction. Shaded areas highlight significant correlations: [$P < 0.05$ (lighter grey), $P < 0.017$ (darker grey, adjusted for multiple comparison), Pearson (partial) correlation].
PPVT = picture-word matching; ACC = anterior cingulate cortex; Calc = calcarine cortex; FI = frontoinsula; Fus = fusiform; MTG = middle temporal gyrus; OFC = orbitofrontal cortex.

sulcus, Heschl's gyrus, precentral and postcentral gyri, and dorsal posterior insula (primary interoceptive cortex)]; association cortices (lingual, lateral occipital, fusiform, superior and middle temporal gyri); and corticoid, allocortical and peri-allocortical regions (amygdala, frontoinsula, orbital frontal cortex, posterior cingulate cortex and parahippocampus/hippocampus) as shown in Fig. 2A ($P < 0.01$ height and $P < 0.05$ cluster extent, Supplementary Table 1). Most regions remained significant after voxel-wise atrophy correction (Supplementary Table 1). No region showed increased ATL connectivity in patients with semantic variant PPA.

To address the possibility that disrupted intrinsic connectivity to the ATL might merely reflect atrophy within the ATL seed regions, we employed a seed-independent, voxel-wise local task-free functional MRI measure: fractional ALFF. This measure quantifies the power of each voxel's low frequency (0.01–0.08 Hz) blood oxygen level-dependent signal oscillations relative to its power across the entire frequency range and thus reflects regional spontaneous brain activity independent from the seed (Zou *et al*., 2008). Comparing patients with controls, we identified a striking pattern of regions with significantly reduced low-frequency blood oxygen level-dependent oscillation power ($P < 0.01$ height and $P < 0.05$ cluster extent; Fig. 2B, Supplementary Table 2) that converged with the patterns of ATL connectivity in the healthy brain (Fig. 1) and reduced ATL connectivity in semantic variant PPA (Fig. 2A and C). Most regions with reduced fractional ALFF remained significant after voxel-wise atrophy correction (Supplementary Table 2). No region was found to have greater low-frequency blood oxygen level-dependent oscillation power in patients with semantic variant PPA compared with control subjects.

Semantic variant primary progressive aphasia-related physiological impairments beyond the anterior temporal lobe correlate with deficits in relevant functional domains

Having demonstrated widely distributed abnormalities in intrinsic connectivity and local low frequency oscillation power in semantic variant PPA, we asked whether these physiological impairments were related to semantic deficits observed in the patients. We hypothesized that impaired local regional function (fractional ALFF) would correlate with semantic deficits in functional domains requiring information processed in those regions. To test this hypothesis, we focused on two neuropsychological tests. First, we chose the Peabody Picture Vocabulary Test, a word-to-picture matching task, for its reliance on semantic processing of auditory, lexical and visual representations (Dunn, 1970); subjects are asked to match a spoken word representing an object, action, or attribute (with neutral emotion) to one of four picture choices. Second, we chose the TASIT Emotion Evaluation Subtest, an emotion–word matching task, for its reliance on semantic representations of emotion; subjects are asked to select a word best matching the emotional state portrayed in a video vignette from seven choices (happy, surprised, sad, anxious, angry, disgusted and neutral) (Mcdonald *et al*., 2007). We predicted that Peabody Picture Vocabulary Test performance would correlate with fractional ALFF values from disrupted posterior visual and language processing areas (most of which were found in the left hemisphere) whereas TASIT performance would correlate with fractional ALFF values from perturbed emotion processing regions (most of which were found in the right hemisphere).

Based on these predictions, we selected two sets of regions of interest from the fractional ALFF group difference map (semantic variant PPA < HC3). Set 1 regions of interest included the left fusiform, middle temporal, and calcarine cortices (Fig. 3A), regions that have been consistently activated during picture naming tasks (Murtha *et al*., 1999; Grossman *et al*., 2004); Set 2 regions of interest included the right frontoinsula, anterior cingulate cortex and orbitofrontal cortex (Fig. 3B), chosen for their involvement in emotion processing (Kringelbach, 2005; Craig, 2009). Consistent with our hypotheses, Peabody Picture Vocabulary Test scores correlated with fractional ALFF values of Set 1 (Fig. 3C) but not Set 2 (Fig. 3D) regions of interest, whereas TASIT scores correlated with fractional ALFF values of Set 2 (Fig. 3F) but not Set 1 (Fig. 3E) regions of interest ($P < 0.05$, Pearson correlation; Table 3). After region of interest-wise atrophy correction, most significant correlations remained ($P < 0.05$, Pearson partial correlation; Table 3). These findings illustrate the functional relevance of semantic variant PPA-related physiological disruptions in specific nodes of the anterior temporal lobe network.

Blood oxygen level-dependent oscillation deficits in upstream auditory versus visual processing regions correlate with dorsal versus ventral anterior temporal lobe atrophy

Human cytoarchitectonic and primate axonal tracer studies have shown that the ATLs contain functionally segregated subregions (Insausti *et al*., 1987*a*, *b*; Blaizot *et al*., 2010). In particular, a dorsal-ventral ATL gradient has been observed wherein the dorsal ATL makes reciprocal connections with upstream auditory areas whereas the ventral ATL is allied with ventral visual

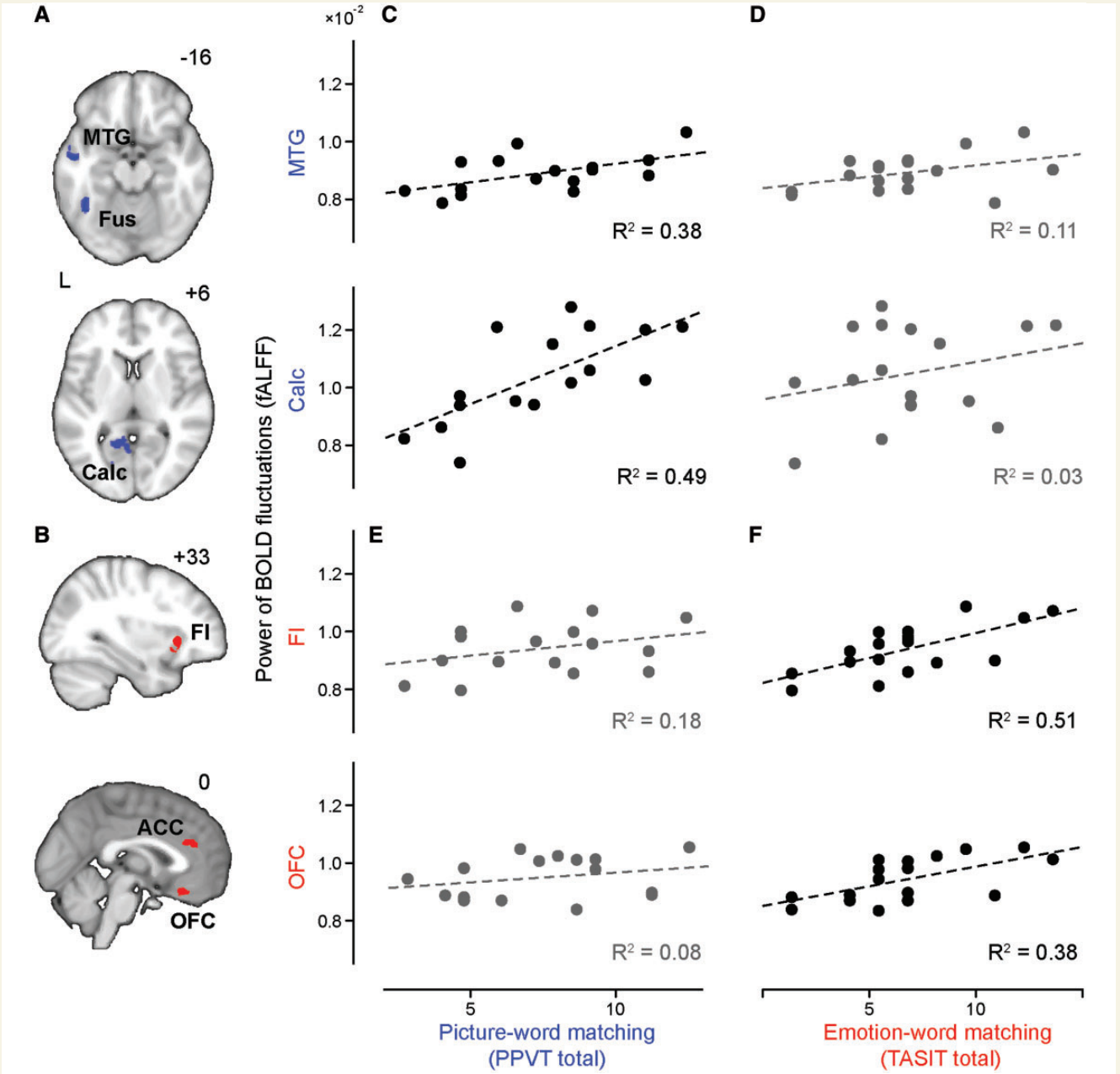

Figure 3 Local functional activity impairments correlate with semantic deficits. Set I (**A**, blue) and Set II (**B**, red) regions of interest were selected from the fractional ALFF semantic variant PPA < HC3 difference map. Mean fractional ALFF values from selected regions of interest were plotted against scores on a semantic processing [Peabody Picture Vocabulary Test (PPVT)]; (**C** and **E**) and emotion recognition (TASIT; **D** and **F**) task. Significant correlations ($P < 0.017$, Pearson correlation, Bonferroni-corrected for multiple comparisons) are plotted in black (**C** and **F**) and non-significant correlations are plotted in grey (**D** and **E**). ACC = anterior cingulate cortex; BOLD = blood oxygen level-dependent; Calc = calcarine; FI = frontoinsula; Fus = fusiform; MTG = middle temporal gyrus.

processing nodes (Fig. 4A) (Morán *et al*., 1987; Olson *et al*., 2007; Ding *et al*., 2009). Accordingly, we hypothesized that damage to dorsal and ventral ATL subregions would differentially impact the physiological integrity of posterior auditory and visual regions. To test this hypothesis, we extracted four regions of interest from each hemisphere, including primary visual cortex (calcarine), primary auditory cortex (Heschl's), visual association cortex (fusiform) and auditory association cortex (superior temporal gyrus), based on the fractional ALFF group difference (semantic variant PPA < HC3) map. The mean fractional ALFF values within these regions of interest were then used to examine whether ipsilateral ATL grey matter atrophy predicted the functional deficits in posterior primary and modality-selective regions.

Because fractional ALFF values within auditory and visual processing regions were mildly collinear (r = 0.3–0.47), we entered these regional fractional ALFF values as orthogonalized covariates in a voxel-based morphometry general linear model to identify ipsilateral ATL voxels whose grey matter intensity correlated with

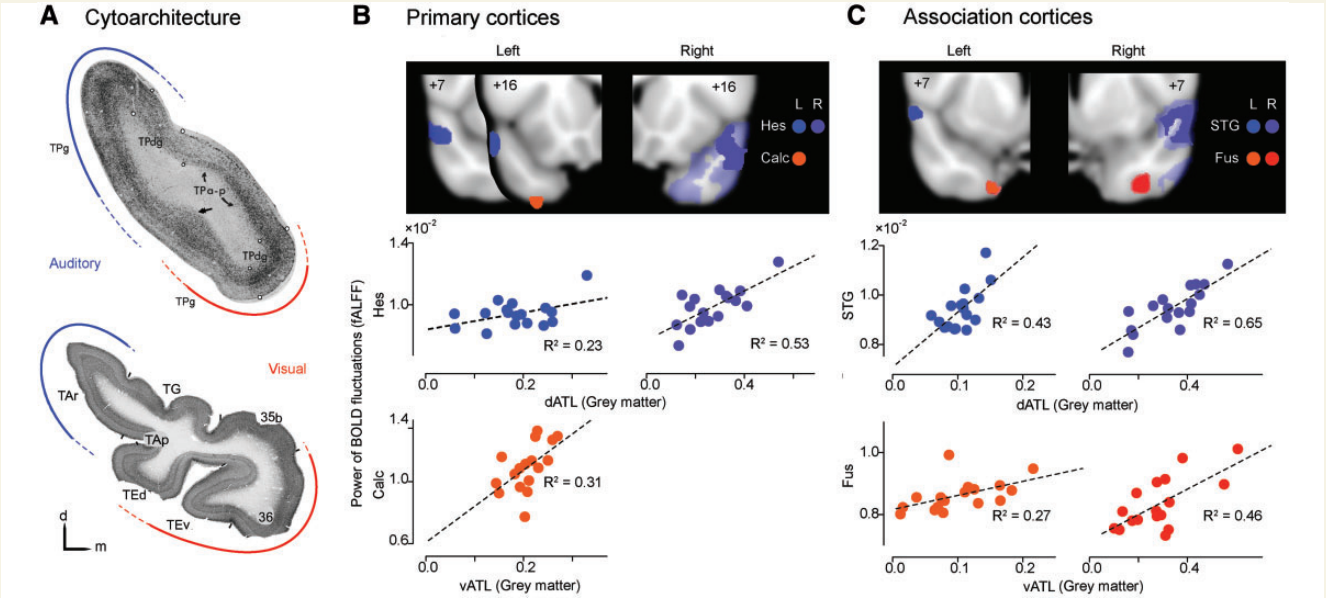

Figure 4 ATL subregion grey matter atrophy predicts fractional ALFF values within visual versus auditory processing regions. (**A**) *Top:* Coronal section through the ATL of the rhesus monkey, showing cytoarchitectural subdivisions [reprinted with permission from Fig. 1 in Morán *et al*., 1987)]. Tract tracing results suggested that auditory inputs predominate in the dorsolateral part of the temporopolar cortex (blue) whereas visual inputs become more prominent in the ventral ATL (red). TPa-p = temporopolar cortex, agranular periallocortical; TPdg = temporopolar cortex, dysgranular; TPg = temporopolar cortex, granular. *Bottom*: Human ATL coronal section illustrating parallel cytoarchitectural subdivisions, reprinted (left–right flipped for comparison) with permission from Fig. 9A in Ding *et al*. (2009). The authors commented (p. 621) that Area TAr is thought to be involved in higher order auditory processing (blue), whereas anterior areas 35, 36, and TE are thought to be involved in high order visual processing (red). TAr = the area rostral to area TA; TAp = the polysensory area in the dorsal bank of the STS; TEd, TEr = dorsal and ventral parts of area TE; TG = the area caps the tip of temporal pole; 35B, 36 = Area 35b and 36 based on Brodmann (Brodmann, 1909). Temporal areas TA and TE are based on Von Ecomono and Koskinas (Von Economo, 1929). Voxel-based regression analyses included (**B**) primary cortices (calcarine sulcus and Heschl's gyrus) and (**C**) sensory association cortices (fusiform and superior temporal gyri). Consistent with connectivity-based predictions, distinct ATL clusters were identified whose grey matter volumes significantly correlated with fractional ALFF values in posterior visual (orange and red) and auditory (blue and purple) processing regions, thresholded at $P < 0.01$. In the right hemisphere model (**A** and **B**, *right*), more expansive clusters were identified at this threshold for auditory regressors (transparent purple) and were further thresholded at $P < 0.005$ (solid purple) to illustrate the region of peak significance. Results for left and right hemispheres are labelled in different colour tones.

the upstream fractional ALFF values. Primary and modality-selective association cortices were analysed in separate models. Four models were examined: primary visual and auditory cortices (one model for left, one for right) and visual and auditory association cortices (left and right). In all but one model, diminished fractional ALFF values within auditory regions preferentially correlated with atrophy in the dorsal ATL, whereas lower fractional ALFF within visual regions preferentially correlated with ventral ATL atrophy (Fig. 4B and C). In the model for primary cortices from the right hemisphere, the right calcarine cortex fractional ALFF value was not correlated with ipsilateral ATL volume. Overall, these findings further show that ATL damage is associated with physiological impairments within anatomically predictable upstream regions.

Discussion

We used a multidisciplinary approach to examine the neural basis of semantic processing, combining structural MRI, task-free functional MRI, and neuropsychological assessments in healthy subjects and patients with semantic variant PPA, the most reliable lesion model for studying the semantic system in humans. In the healthy brain, the ATLs were intrinsically connected to primary and modality-selective association cortices as well as anterior cingulate, orbitofrontal, and frontoinsular cortices and striatal and thalamic regions. In patients with semantic variant PPA, these regions showed reduced ATL connectivity and blood oxygen level-dependent oscillation power. Regional physiological impairments correlated with domain-relevant neuropsychological deficits. Finally, damage to ATL subregions with known modality-selective cortical connections predicted physiological disruption within the relevant posterior sensory cortices. Taken together, these findings provide novel neurophysiological evidence for the previously proposed model of the semantic network in humans that features a critical, transmodal ATL semantic hub positioned to integrate functionally relevant and topographically organized links to distributed modality-selective regions (Patterson *et al*., 2007).

The controversy regarding the neural representation of semantic knowledge first regarded whether semantics required a critical 'hub' that integrates information coming from modality-selective

regions. Neuropsychological evidence from patients with semantic variant PPA demonstrated that patients with ATL damage have multimodal semantic breakdown, establishing the role of this region as a semantic hub. A cognitive model including a hub interacting with modality-selective regions was then proposed but lacked neurophysiological evidence showing intrinsic functional connectivity between the ATL and modality-selective areas. Here, using task-free functional MRI, we identified robust intrinsic connections between the ATLs and a host of primary and modality-selective upstream regions; these functional links provide the basis for the proposed integrated semantic network, including a hub (or hubs), distributed domains, and most importantly, organized communications between these network nodes (McClelland and Rogers, 2003; Patterson *et al*., 2007).

Our data further illustrate important ATL connections to limbic and peri-allocortical structures that represent stimulus salience and value. Making use of these diverse connections, this ATL-anchored network may orchestrate the integrated decoding and appraisal of ambient stimuli into a scene optimized for behavioural guidance (Simmons *et al*., 2010). Semantic meaning proves most useful when it goes beyond integration of sensory inputs from extrapersonal space to include appraisal of stimulus relevance to intrapersonal space. We hypothesize that the anterior temporal lobe semantic network described here orchestrates these interactions to provide a rich and value-laden contextual landscape for guiding behaviour. These potential ATL-mediated links between value and meaning can now be explored in future studies.

The concept of the ATL as a semantic hub overlaps with the idea of multimodal 'convergence zones' long hypothesized in the neuroscience and cognitive psychology literatures (Geschwind, 1965; Damasio, 1989; Hart and Gordon, 1992; Damasio *et al*., 1996; Mesulam, 1998; Grossman *et al*., 2002; Beauchamp *et al*., 2004). Damasio *et al*. (1996) described the necessity of such convergence zones, which host unified representations extracted from modality-selective regions, for semantic processing. Their framework argued for the existence of multiple specialized convergence regions that integrate information about specific exemplars, or 'unique' items, such as famous faces. Our data suggest that focal atrophy most severe in the ATL can disrupt physiological integrity within diverse regions that span modalities and categories, as proposed by Patterson *et al*. (2007).

Previous magnetic resonance and PET imaging studies in semantic variant PPA have focused on the circumscribed ATL damage seen in these patients (Mummery *et al*., 2000; Rosen *et al*., 2002; Diehl *et al*., 2004), although some studies reported functional impairments that extended into the posterior temporal lobe (Mummery *et al*., 1999). Seeking to reconcile the focal injury in semantic variant PPA with the multimodal semantic deficits observed, Patterson *et al*. (2007) proposed that the critical nature of the ATL reflects its role as an amodal integrative semantic hub that links multimodal representations about a given semantic construct. Our findings provide direct experimental support for this framework by showing, for the first time, widely distributed neurophysiological deficits in semantic variant PPA within regions intrinsically connected to the ATL. Patient performance on semantic tasks was linked to reduced low frequency blood oxygen level-dependent oscillation power within task domain-relevant regions. These findings suggest that focal ATL damage produces physiological deficits extending beyond the ATLs and that this dysfunction is related to the semantic impairment in semantic variant PPA. This conceptualization aligns with aspects of the 'embodied cognition' model by emphasizing the importance of modality-selective primary and association cortices in semantic representations (Martin, 1998; Mahon and Caramazza, 2008). Our semantic variant PPA findings, on the other hand, illustrate that the ATL proves critical for maintaining function within modality-selective regions, most likely by associating modality-specific features to create unitary, modality-independent concepts. These observations support the view that the ATL acts as a key integration centre (or 'hub') used to maintain interactions among spatially distant perceptual and linguistic representations. Lack of communication with the ATL hub could cause a functional diaschisis (Price *et al*., 2001) that leads to impaired physiological integrity of modality-selective regions.

This study further suggests that the ATLs process lateralized and topographically organized representations, as has been suggested previously (Poremba *et al*., 2004; Skipper *et al*., 2011; Gainotti, 2012). Patients with semantic variant PPA, including those studied here, often show asymmetric ATL atrophy, with left-predominant atrophy accompanied by greater general semantic impairment and right-predominant atrophy favouring social–emotional deficits (Thompson *et al*., 2003; Seeley *et al*., 2005). The left and right ATLs may receive and process related but distinct incoming sensory inputs that shape the concepts represented by each ATL. The left ATL, for example, may receive disproportionate inputs from left hemisphere lexical and phonological centres supporting word processing. This model received preliminary support from our observation that Peabody Picture Vocabulary Test performance correlated with physiological integrity in these regions. The right ATL, in contrast, may receive disproportionate inputs from right-lateralized emotion processing structures such as the orbitofrontal cortex, frontoinsula and anterior cingulate cortex, explaining the relationship identified here between physiological integrity of these structures and emotion comprehension. Our data also support regional subdivisions within the ATLs. In patients with semantic variant PPA, dorsal ATL atrophy preferentially correlated with physiological dysfunction in posterior auditory cortices, whereas ventral ATL degeneration predicted posterior visual area dysfunction. These findings converge with data concerning the topographical organization of the ATL in humans and monkeys, suggesting that the human ATL contains both integrated and modality-selective subregions (Morán *et al*., 1987; Ding *et al*., 2009; Skipper *et al*., 2011). More importantly, the findings further detail how focal ATL damage undermines upstream modality-selective cortex integrity.

Limitations

The current study has two chief limitations. First, although we took extensive steps to diminish the influence of brain atrophy on our functional imaging data, it remains possible that structural neurodegeneration affected intrinsic connectivity in posterior nodes of the semantic network. Many regions in which we found reduced ATL connectivity and local blood oxygen level-

dependent oscillation power, however, have shown striking structural integrity in patients with semantic variant PPA, especially in the earlier disease stages (Gorno-Tempini *et al*., 2004; Sapolsky *et al*., 2010; Acosta-Cabronero *et al*., 2011). Whether these regions harbour incipient neuropathology or falter solely due to ATL injury remains a topic for future study. Second, an extensive battery of semantic tests covering all major sensory modalities was not available for our semantic variant PPA group, and task-free functional MRI controls (HC3) underwent only a subset of the semantic battery used in semantic variant PPA subjects. Comprehensive semantic batteries prove unfeasible for some patients and are not required to make a diagnosis of semantic variant PPA, in part because patients meeting semantic variant PPA diagnostic criteria (with word and object knowledge deficits) have been shown to exhibit multimodal semantic deficits (Garrard and Hodges, 2000; Patterson *et al*., 2007). Nevertheless, data from a broader range of modality-specific tasks would have enabled more direct testing of some of our function–behaviour correlation hypotheses.

Conclusion

We provided neurophysiological evidence supporting the view that semantic processing is orchestrated through functionally relevant and topographically organized interactions between a critical ATL hub and modality-selective processing regions. The findings may help guide further studies toward understanding semantic processing in the human brain in health and disease.

Acknowledgements

We thank Paul Keselman, Lara Stables, Sebastian Dionisio, and William Irwin for technical assistance with data collection and storage. We thank our patients and their families for their invaluable contributions to neurodegenerative disease research.

Funding

This work was supported by the National Institute of Aging (NIA grants AG19724 and AG1657303 to B.L.M. and W.W.S.), the National Institute of Neurological Diseases and Stroke (NS050915 grant to M.L.G.T) the Larry L. Hillblom Foundation (J.H.K.), Marie Curie International Grant (MIRG-CT- 2007-046512 to M.L.G.T.), Provincia Autonoma di Trento, Fondazione Cassa di Risparmio di Trento e Rovereto, Italy.

Supplementary material

Supplementary material is available at *Brain* online.

References

Acosta-Cabronero J, Patterson K, Fryer TD, Hodges JR, Pengas G, Williams GB, et al. Atrophy, hypometabolism and white matter abnormalities in semantic dementia tell a coherent story. Brain 2011; 134: 2025–35.

Beauchamp MS, Argall BD, Bodurka J, Duyn JH, Martin A. Unraveling multisensory integration: patchy organization within human STS multisensory cortex. Nature Neuroscience 2004; 7: 1190–2.

Beeson PM, Rising K, Kim ES, Rapcsak SZ. A treatment sequence for phonological alexia/agraphia. J Speech Lang Hear Res 2010; 53: 450–68.

Binder JR, Desai RH, Graves WW, Conant LL. Where is the semantic system? A critical review and meta-analysis of 120 functional neuroimaging studies. Cereb Cortex 2009; 19: 2767–96.

Blaizot X, Mansilla F, Insausti AM, Constans JM, Salinas-Alamán A, Pró-Sistiaga P, et al. The human parahippocampal region: I. Temporal pole cytoarchitectonic and MRI correlation. Cereb Cortex 2010; 20: 2198–212.

Brodmann K. Vergleichende lokalisationslehre der Grosshirnrinde. Leipzig: Barth; 1909.

Casanova R, Srikanth R, Baer A, Laurienti PJ, Burdette JH, Hayasaka S, et al. Biological parametric mapping: a statistical toolbox for multimodality brain image analysis. NeuroImage 2007; 34: 137–43.

Castellanos FX, Kelly C, Milham MP. The restless brain: attention-deficit hyperactivity disorder, resting-state functional connectivity, and intra-subject variability. Can J Psychiatry 2009; 54: 665–72.

Chan D, Fox NC, Scahill RI, Crum WR, Whitwell JL, Leschziner G, et al. Patterns of temporal lobe atrophy in semantic dementia and Alzheimer's disease. Ann Neurol 2001; 49: 433–42.

Craig AD. How do you feel? Interoception: the sense of the physiological condition of the body. Nat Rev Neurosci 2002; 3: 655–66.

Craig AD. How do you feel–now? The anterior insula and human awareness. Nat Rev Neurosci 2009; 10: 59–70.

Damasio AR. Time-locked multiregional retroactivation: a systems-level proposal for the neural substrates of recall and recognition. Cognition 1989; 33: 25–62.

Damasio H, Grabowski TJ, Tranel D, Hichwa RD, Damasio AR. A neural basis for lexical retrieval. Nature 1996; 380: 499–505.

Desgranges B, Matuszewski V, Piolino P, Chételat G, Mézenge F, Landeau B, et al. Anatomical and functional alterations in semantic dementia: a voxel-based MRI and PET study. Neurobiol Aging 2007; 28: 1904–13.

Diehl J, Grimmer T, Drzezga A, Riemenschneider M, Förstl H, Kurz A. Cerebral metabolic patterns at early stages of frontotemporal dementia and semantic dementia. A PET study. Neurobiol Aging 2004; 25: 1051–6.

Van Dijk KR, Sabuncu MR, Buckner RL. The influence of head motion on intrinsic functional connectivity MRI. Neuroimage 2011; 59: 1–8.

Ding SL, Van Hoesen GW, Cassell MD, Poremba A. Parcellation of human temporal polar cortex: a combined analysis of multiple cytoarchitectonic, chemoarchitectonic, and pathological markers. J Comp Neurol 2009; 514: 595–623.

Dunn LM. Expanded manual for the Peabody Picture Vocabulary Test. Minneapolis, MN: American Guidance Service; 1970.

Von Economo C. The cytoarchitectonics of the human cerebral cortex. London: Oxford University Press; 1929.

Gainotti G. The format of conceptual representations disrupted in semantic dementia: a position paper. Cortex 2011: p. 521–9.

Garrard P, Hodges JR. Semantic dementia: clinical, radiological and pathological perspectives. J Neurol 2000; 247: 409–22.

Geschwind N. Disconnexion syndromes in animals and man. I. Brain 1965; 88: 237–94.

Gesierich B, Jovicich J, Riello M, Adriani M, Monti A, Brentari V, et al. Distinct neural substrates for semantic knowledge and naming in the temporoparietal network. Cereb Cortex 2012; 22: 2217–26.

Gorno-Tempini ML, Dronkers NF, Rankin KP, Ogar JM, Phengrasamy L, Rosen HJ, et al. Cognition and anatomy in three variants of primary progressive aphasia. Ann Neurol 2004; 55: 335–46.

Gorno-Tempini ML, Hillis AE, Weintraub S, Kertesz A, Mendez M, Cappa SF, et al. Classification of primary progressive aphasia and its variants. Neurology 2011; 76: 1006–14.

Greicius M. Resting-state functional connectivity in neuropsychiatric disorders. Curr Opin Neurol 2008; 21: 424–30.

Grossman M, Smith EE, Koenig P, Glosser G, DeVita C, Moore P, et al. The neural basis for categorization in semantic memory. NeuroImage 2002; 17: 1549–61.

Grossman M, McMillan C, Moore P, Ding L, Glosser G, Work M, et al. What's in a name: voxel-based morphometric analyses of MRI and naming difficulty in Alzheimer's disease, frontotemporal dementia and corticobasal degeneration. Brain 2004; 127: 628–49.

Guo CC, Kurth F, Zhou J, Mayer EA, Eickhoff SB, Kramer JH, et al. One-year test-retest reliability of intrinsic connectivity network fMRI in older adults. NeuroImage 2012; 61: 1471–83.

Hart J Jr, Gordon B. Neural subsystems for object knowledge. Nature 1992; 359: 60–4.

Howard D, Patterson KE. The Pyramids and Palm Trees Test: a test of semantic access from words and pictures. Bury St Edmunds. Suffolk: Thames Valley Test Company; 1992.

Insausti R, Amaral DG, Cowan WM. Entorhinal cortex of the monkey: II. Cortical afferents. J Comp Neurol 1987a; 264: 356–95.

Insausti R, Amaral DG, Cowan WM. Entorhinal cortex of the monkey: III. Subcortical afferents. J Comp Neurol 1987b; 264: 396–408.

Kaplan EF, Goodglass H, Weintraub S. The Boston naming test. Philadelphia, PA: Lea & Febiger; 1983.

Kringelbach M. The human orbitofrontal cortex: linking reward to hedonic experience. Nat Rev Neurosci 2005; 6: 691–702.

Mahon BZ, Caramazza A. A critical look at the embodied cognition hypothesis and a new proposal for grounding conceptual content. J Physiol Paris 2008; 102: 59–70.

Maldjian JA, Laurienti PJ, Kraft RA, Burdette JH. An automated method for neuroanatomic and cytoarchitectonic atlas-based interrogation of fMRI data sets. NeuroImage 2003; 19: 1233–9.

Martin A. Organization of semantic knowledge and the origin of words in the brain. The Origin and Diversification of Language. San Francisco, CA: California Academy of Sciences; 1998, p. 69–98.

Martin A. The representation of object concepts in the brain. Ann Rev Psychol 2007; 58: 25–45.

McClelland JL, Rogers TT. The parallel distributed processing approach to semantic cognition. Nat Rev Neurosci 2003; 4: 310–22.

Mcdonald S, Flanagan S, Rollins J. The Awareness of Social Inference Test (TASIT). Bury St Edmonds, UK: Thames Valley Test Company; 2007.

Mesulam M. From sensation to cognition. Brain 1998; 121 (Pt. 6): 1013–52.

Mesulam MM. Principles of behavioral and cognitive neurology. New York, NY: Oxford University Press; 2000.

Morán MA, Mufson EJ, Mesulam MM. Neural inputs into the temporopolar cortex of the rhesus monkey. J Comp Neurol 1987; 256: 88–103.

Mummery CJ, Patterson K, Wise RJ, Vandenberghe R, Vandenbergh R, Price CJ, et al. Disrupted temporal lobe connections in semantic dementia. Brain 1999; 122: 61–73.

Mummery CJ, Patterson K, Price CJ, Ashburner J, Frackowiak RS, Hodges JR. A voxel-based morphometry study of semantic dementia: relationship between temporal lobe atrophy and semantic memory. Ann Neurol 2000; 47: 36–45.

Murtha S, Chertkow H, Beauregard M, Evans A. The neural substrate of picture naming. J Cogn Neurosci 1999; 11: 399–423.

Olson IR, Plotzker A, Ezzyat Y. The enigmatic temporal pole: a review of findings on social and emotional processing. Brain 2007; 130: 1718–31.

Patterson K, Nestor PJ, Rogers TT. Where do you know what you know? The representation of semantic knowledge in the human brain. Nat Rev Neurosci 2007; 8: 976–87.

Pievani M, De Haan W, Wu T, Seeley WW, Frisoni GB. Functional network disruption in the degenerative dementias. Lancet Neurol 2011; 10: 829–43.

Poline JB, Worsley KJ, Evans AC, Friston KJ. Combining spatial extent and peak intensity to test for activations in functional imaging. Neuroimage 1997; 5: 83–96.

Poremba A, Malloy M, Saunders R, Carson R. Species-specific calls evoke asymmetric activity in the monkey's temporal poles. Nature 2004; 427: 448–51.

Price CJ, Warburton EA, Moore CJ, Frackowiak RS, Friston KJ. Dynamic diaschisis: anatomically remote and context-sensitive human brain lesions. J Cogn Neurosci 2001; 13: 419–29.

Rankin KP, Salazar A, Gorno-Tempini ML, Sollberger M, Wilson SM, Pavlic D, et al. Detecting sarcasm from paralinguistic cues: anatomic and cognitive correlates in neurodegenerative disease. NeuroImage 2009; 47: 2005–15.

Robinson S, Basso G, Soldati N, Sailer U, Jovicich J, Bruzzone L, et al. A resting state network in the motor control circuit of the basal ganglia. BMC Neurosci 2009; 10: 137.

Rosen HJ, Gorno-Tempini ML, Goldman WP, Perry RJ, Schuff N, Weiner M, et al. Patterns of brain atrophy in frontotemporal dementia and semantic dementia. Neurology 2002; 58: 198–208.

Sapolsky D, Bakkour A, Negreira A, Nalipinski P, Weintraub S, Mesulam MM, et al. Cortical neuroanatomic correlates of symptom severity in primary progressive aphasia. Neurology 2010; 75: 358–66.

Seeley WW, Bauer AM, Miller BL, Gorno-Tempini ML, Kramer JH, Weiner M, et al. The natural history of temporal variant frontotemporal dementia. Neurology 2005; 64: 1384–90.

Seeley WW, Crawford RK, Zhou J, Miller BL, Greicius MD. Neurodegenerative diseases target large-scale human brain networks. Neuron 2009; 62: 42–52.

Simmons WK, Reddish M, Bellgowan PS, Martin A. The selectivity and functional connectivity of the anterior temporal lobes. Cereb Cortex 2010; 20: 813–25.

Skipper LM, Ross LA, Olson IR. Sensory and semantic category subdivisions within the anterior temporal lobes. Neuropsychologia 2011; 49: 3419–29.

Thompson SA, Patterson K, Hodges JR. Left/right asymmetry of atrophy in semantic dementia: behavioral-cognitive implications. Neurology 2003; 61: 1196–203.

Vincent JL, Patel GH, Fox MD, Snyder AZ, Baker JT, Van Essen DC, et al. Intrinsic functional architecture in the anaesthetized monkey brain. Nature 2007; 447: 83–6.

Zhang S, Li CS. A neural measure of behavioral engagement: task-residual low-frequency blood oxygenation level-dependent activity in the precuneus. Neuroimage 2010; 49: 1911–8.

Zou QH, Zhu CZ, Yang Y, Zuo XN, Long XY, Cao QJ, et al. An improved approach to detection of amplitude of low-frequency fluctuation (ALFF) for resting-state fMRI: fractional ALFF. J Neurosci Methods 2008; 172: 137–41.